CrossMark

MAGNETIC RESONANCE

Contribution of mono-exponential, bi-exponential and stretched exponential model-based diffusion-weighted MR imaging in the diagnosis and differentiation of uterine cervical carcinoma

Meng Lin[1] · Xiaoduo Yu[1] · Yan Chen[1] · Han Ouyang[1] · Bing Wu[2] · Dandan Zheng[2] · Chunwu Zhou[1]

Abstract

Objectives To investigate the potential of various metrics derived from mono-exponential model (MEM), bi-exponential model (BEM) and stretched exponential model (SEM)-based diffusion-weighted imaging (DWI) in diagnosing and differentiating the pathological subtypes and grades of uterine cervical carcinoma.

Methods 71 newly diagnosed patients with cervical carcinoma (50 cases of squamous cell carcinoma [SCC] and 21 cases of adenocarcinoma [AC]) and 32 healthy volunteers received DWI with multiple b values. The apparent diffusion coefficient (ADC), pure molecular diffusion (D), pseudo-diffusion coefficient ($D*$), perfusion fraction (f), water molecular diffusion heterogeneity index (alpha), and distributed diffusion coefficient (DDC) were calculated and compared between tumour and normal cervix, among different pathological subtypes and grades.

Results All of the parameters were significantly lower in cervical carcinoma than normal cervical stroma except alpha. SCC showed lower ADC, D, f and DDC values and higher $D*$ value than AC; D and DDC values of SCC and ADC and D values of AC were lower in the poorly differentiated group than those in the well–moderately differentiated group.

Conclusion Compared with MEM, diffusion parameters from BEM and SEM may offer additional information in cervical carcinoma diagnosis, predicting pathological tumour subtypes and grades, while f and D showed promising significance.

Key Points
- *DWI-derived parameters by different models are related but provide diversified information.*
- *Commonly used ADC by MEM of DWI overestimates the tissue water diffusivity.*
- *DWI processed by BEM could separate blood perfusion from true diffusion effects.*
- *The derived diffusion-related and perfusion-related parameters by BEM are superior to ADC.*

✉ Han Ouyang
houybj@126.com

[1] Department of Diagnostic Radiology, Cancer Institute & Hospital, Peking Union Medical College, Chinese Academy of Medical Sciences, No17, Panjiayuannanli, Chaoyang District, Beijing 100021, People's Republic of China

[2] GE MR Research China, Beijing, People's Republic of China

Abbreviations

AC	Adenocarcinoma
ADC	Apparent diffusion coefficient
Alpha	Water molecular diffusion heterogeneity index
BEM	Bi-exponential model
D	Pure molecular diffusion
$D*$	Pseudo-diffusion coefficient
DCE-MRI	Dynamic contrast-enhanced MRI
DDC	Distributed diffusion coefficient
DWI	Diffusion-weighted imaging
f	Perfusion fraction
MEM	Mono-exponential model
MRI	Magnetic resonance imaging
SCC	Squamous cell carcinoma
SEM	Stretched exponential model

Introduction

The prognostic factors of uterine cervical carcinoma include tumour volume, stage, pathological subtype and grade, status of lymph node, etc. [1, 2]. MRI provides excellent morphological information for cervical carcinoma. MRI methods such as diffusion-weighted imaging (DWI) and dynamic contrast-enhanced MRI (DCE-MRI), which respectively reflect the water molecule diffusion and perfusion process, may help not only in tumour diagnosis, stage and therapeutic effect evaluation but also in tumour subtype classification, grade distinguishing and therapeutic outcome prediction [3–10]. DCE-MRI requires intravenous administration that may be associated with danger such as allergy and nephrogenic systemic fibrosis (NSF), whereas DWI remains completely non-invasive.

To date, apparent diffusion coefficient (ADC) is the most commonly used metric in the mono-exponential model (MEM) of DWI; however, it does not consider the influence of the microcirculation of blood in capillaries, which may lead to inaccurate description of the diffusion. On the other hand, the bi-exponential model (BEM) separates blood perfusion from true diffusion effects and leads to diffusion-related parameters D (pure molecular diffusion) and perfusion-related parameters including D^* (pseudo-diffusion coefficient) and f (perfusion fraction). Several studies have investigated the relationship between these metrics and those from DCE-MRI [11–17] and concluded that the BEM-derived metrics might be superior to ADC in tumour diagnosis and pathological grade prediction [12, 18–20]. Only limited cases of BEM DWI application in cervical carcinoma have been reported so far and these were mainly focused on the comparison with DCE-MRI in tissue differentiation including tumour, normal cervix, myometrium and leiomyoma [15, 21]. However, the use of BEM in pathological subtype classification and grade identification has not been investigated.

The stretched exponential model (SEM) was initially introduced by Bennett et al. [22, 23] to evaluate diffusion and intravoxel heterogeneity, as represented by the parameters of DDC (distributed diffusion coefficient) and alpha (water diffusion heterogeneity index). SEM has been applied in malignant tumours such as gliomas [24], nasopharyngeal carcinoma (NPC) [25], prostate [26–28], and ovarian tumours [29]; SEM has been demonstrated to be superior to MEM and BEM in certain cancer types, such as prostate and ovarian [27–29], and superior to MEM in glioma grading [24]. The application of SEM in cervical carcinoma is still lacking.

This current study aims to extend the application of BEM and SEM, in addition to MEM, in cervical carcinoma to investigate the potential of various parameters in tumour diagnosis and identification of pathological subtypes and grades.

Materials and methods

Patients

This prospective study was approved by the institutional review board and informed consent was obtained from all patients and healthy volunteers before MRI examinations. A total of 82 patients with newly diagnosed cervical carcinomas proved by preliminary pathology were initially enrolled. Out of the total 82 cases, 51 cases of squamous cell carcinoma (SCC) were collected in the period of March to September 2014, 28 cases of adenocarcinoma (AC) were collected in the period of March 2014 to May 2015, and three cases of rare pathological subtypes including small cell carcinoma ($n = 1$) and adenosquamous carcinoma ($n = 2$) confirmed by further pathological review or rebiopsy. Eight cases (one SCC and seven AC) were excluded because of insignificant lesion dimension (less than 1.0 cm) that may influence the measurement accuracy; the three rare subtype cases were also excluded. In the end, 71 cases of cervical carcinomas were enrolled in this study (age range 25–73 years, median age 46 years; lesion maximum diameter 1.1–8 cm, mean 3.73 cm), comprising 50 cases of SCC (18 cases were poorly differentiated, 19 cases were moderately differentiated, seven cases were well differentiated and six cases were of unknown differentiation as a result of insignificant biopsy specimens size) and 21 cases of AC (six cases were poorly differentiated, eight cases were moderately differentiated, six cases were well differentiated, one case was of unknown differentiation as a result of small biopsy specimens size; the subtype of AC was further identified as endocervical type in 12 cases, endometrioid in five cases, gastric-type mucinous type in three cases, mesonephric type in one case). Twenty-five cases were in clinical FIGO stage IB, five cases were in stage IIA, 16 cases were in stage IIB, 23 cases were in stage IIIB, and two cases were in stage IVA. For treatment, 28 cases were treated by radical hysterectomy, 36 cases were treated by concurrent chemoradiotherapy and seven cases did not received therapy in our hospital. In addition, 32 age-matched healthy volunteers (age range 28–61 years, median 45 years), without gynaecological disease or history of carcinoma, were recruited as a control group in this study.

Magnetic resonance imaging

MRI examinations were performed on a 3-T whole body scanner (Discovery 750, GE Healthcare, US) with an 8-channel phase array coil. Conventional non-enhanced series were conducted on all patients and healthy volunteers, including axial fast recovery fast spin echo (FRFSE) sequence T1WI (TR/TE = 620 ms/ 8.2 ms, slice thickness/slice gap = 5 mm/1 mm); FRFSE T2WI axial (TR/TE = 360 ms/130.0 ms, slice thickness/slice gap = 4 mm/0.4 mm); FRFSE T2WI sagittal (TR/ TE = 5620 ms/135.6 ms, slice thickness/slice gap = 4 mm/ 0.4 mm); axial pre-saturated fat suppression FRFSE T2WI

sequence (TR/TE = 5100 ms/106.6 ms, slice thickness/slice gap = 5 mm/1 mm). Conventional DWI (single-shot echo-planar imaging [SE-EPI], TR/TE = 5500 ms/62.7 ms, slice thickness/slice gap = 5 mm/1 mm, number of excitations (NEX) = 2, matrix = 128 × 128, b value = 0 and 800 s/mm^2, acquisition time [TA] = 1 min).

The multiple-b-value DWI: SE-EPI, using the same spatial coverage to that of non-enhanced axial pre-saturated fat suppression FRFSE T2WI sequence, TR/TE 4000 ms/70 ms, slice thickness = 5 mm, slice gap = 1 mm, field of view (FOV) = 34 cm, bandwidth = 250 Hz/pixel, matrix = 128 × 128, parallel imaging factor of 2, TA = 6 min, 13 b values (NEX) : 0 (2),10 (2),25 (2),50 (2),75 (2),100 (1),150 (1),200 (1),400 (1),800 (1),1000 (4),1500 (6),2000 (6) s/mm^2.

Contrast-enhanced images were also acquired after contrast administration (0.2 mmol/kg body weight Gd-DTPA, at rate of 2.0 ml/s, followed by saline flush of 20 ml), imaging series included sagittal or axial DCE-MRI (TR/TE = 3.9 ms/1.8 ms, slice thickness/slice gap = 3 mm/0 mm, acquisition time = 240 s), single-phase sagittal, axial and coronal enhanced series (TR/TE = 3.7 ms/1.7 ms, slice thickness/slice gap = 3 mm/0 mm). All the patients received a contrast-enhanced scan except two patients as a result of a history of allergy. The control group did not receive an enhanced scan.

Data analysis

All DW images were anonymized and de-identified prior to data analysis and then processed using the Advantage Workstation (ADW 4.6 version, GE, US). Two observers with 22 years (O.H.) and 10 years (X.Y.) of experience in body tumour MRI were blinded to the patients' information and individually measured the resulting parameter maps. For the patient group, the slice with maximal tumour dimension was selected; then the regions of interest (ROIs) containing all the tumour region and avoiding obvious necrotic areas were manually delineated, and both non-enhanced and contrast-enhanced series were used as reference to determine the tumour extent; for the control group, the slice with maximal area of cervix was selected and ROIs including all the cervical stroma and excluding the mucosa were identified. Parametric maps were generated according to the following:

(1) Mono-exponential model:

$$S(b)/S_0 = \exp(-b \times \text{ADC})$$

where $S(b)$ is the mean signal intensity with diffusion gradient b, and S_0 is the mean signal intensity without diffusion gradient.

(2) Bi-exponential model:

$$S(b)/S_0 = (1-f)\exp(-b \times D) + f\exp(-b \times D^*)$$

where D is the pure molecular diffusion. D^* is the pseudo-diffusion coefficient, f is the microvascular volume fraction representing the fraction of diffusion linked to microcirculation.

(3) Stretched exponential model:

$$S(b)/S_0 = \exp\left[-(b \times \text{DDC})^{\text{alpha}}\right]$$

where DDC (distributed diffusion coefficient) is the distributed diffusion coefficient reflecting the mean intravoxel diffusion rate, and alpha (water diffusion heterogeneity index) corresponds to intravoxel water diffusion heterogeneity ranging between 0 and 1 [25].

Statistical analysis

SPSS Statistics version 18.0 (v. 18.0, Chicago, IL) and MedCalc 13.0.4.0 (MedCalc, Mariakerke, Belgium) were used for statistical analysis. A two-way model average measure intraclass correlation coefficient (ICC) was used to test the interobserver consistency. Then all the measurements from the two observers were averaged for further comparison. The Kolmogorov–Smirnov test was conducted to analyse the normal distribution of all metrics. Comparisons between tumour and normal cervix, between different pathological subtypes and grades were performed by independent t test (D, D^* and alpha, which conformed to normal distribution) and Mann–Whitney U test (f and DDC, which did not conform to normal distribution). Spearman correlation analysis was used to examine the relationship among different parameters for tumour staging. The area under the curve (AUC) of the receiver operating characteristic (ROC) curve for the significant parameters was calculated and compared by MedCalc. P values of less than 0.05 were considered as statistically significant.

Results

The outcomes of the proposed statistical comparisons are listed as follows. *Interobserver*: Good agreement between measurements from two observers with remarkably high ICC values (0.921–0.980) (Table 1) was obtained. *Tumour and control group*: All the metrics showed significant differences between patient and control group with all P value less

Table 1 Interobserver consistency

	ICC	95 % confidence interval
ADC ($\times 10^{-3}$ mm^2/s)	0.980	0.970–0.986
D ($\times 10^{-3}$ mm^2/s)	0.951	0.927–0.967
D^* ($\times 10^{-3}$ mm^2/s)	0.921	0.883–0.946
f (%)	0.975	0.964–0.983
DDC ($\times 10^{-3}$ mm^2/s)	0.977	0.966–0.984
Alpha	0.969	0.954–0.979

ICC intraclass correlation coefficient

than 0.001 and AUCs of 0.734–0.989, which were lower in cervical carcinoma than normal cervical stroma, except for alpha (Table 2). The AUC of f was the highest with significant difference compared to those of ADC and DDC ($P = 0.004$ and 0.010 respectively). The AUC of DDC was higher than that of ADC but showed no statistical difference ($P = 0.660$) (Fig. 1). *Pathological subtypes*: Cervical SCC showed lower ADC, D, f and DDC values ($P < 0.001$, AUC 0.896–0.950) and higher D^* value ($P = 0.011$, AUC = 0.717) than AC (Table 3) with statistical significance. The AUC of DDC was slightly higher than that of ADC but showed no statistical difference ($P = 0.958$) (Fig. 1). *Pathological grades*: As show in Table 4, D value distinguished pathological grades in both SCC and AC groups ($P = 0.037$, 0.034, respectively); besides,

statistical differences between those two groups were observed for the DDC value of SCC ($P = 0.045$) and ADC value of AC ($P = 0.045$); however, no statistical difference on ROC comparison was seen between D and DDC of SCC and between D and ADC of AC ($P = 0.942$ and 0.611, respectively) (Fig. 1). Other parameters did not demonstrate discrimination performance with statistical significance. In addition, it was observed that none of the measured metrics showed correlation with different tumour stages. Representative examples of the images of normal cervix of healthy volunteers, SCC and AC are shown in Figs. 2, 3, 4, and 5.

Discussion

MEM, BEM and SEM are all based on standard DWI, but with varying underlying models and governing parameters. The applicability of individual models for specific diagnosis purposes is of great interest for their widespread clinical use. In this investigational study, the b values used were carefully chosen to facilitate the derivation of parameters for each of the models [30]. Specifically, a total of 13 b values were chosen including nine in the low range (0, 10, 25, 50, 75, 100, 150, 200, 400 s/mm^2), two in the mid-range (800, 1000 s/mm^2) and two high b values (1500, 2000 s/mm^2), different numbers of excitation were

Table 2 Comparison between tumour and control groups

	Cervical carcinoma ($n = 71$)	Normal cervix stroma ($n = 32$)	P	t/z	AUC	P value of ROC curves comparison
ADC ($\times 10^{-3}$ mm^2/s)	0.87 ± 0.15	1.19 ± 0.16	**<0.001**	9.820 [a]	**0.925**	
D ($\times 10^{-3}$ mm^2/s)	0.67 ± 0.11	0.77 ± 0.13	**<0.001**	4.109[a]	0.739	
D^* ($\times 10^{-3}$ mm^2/s)	11.51 ± 5.22	16.02 ± 5.91	**<0.001**	3.886[a]	0.734	
f (%)	25.11 ± 5.73	46.83 ± 7.78	**<0.001**	−7.918 [b]	**0.989**	0.004 (0.020–0.107) [c]
						0.010 (0.014–0.101) [d]
DDC ($\times 10^{-3}$ mm^2/s)	0.97 ± 0.25	1.74 ± 0.50	**<0.001**	−7.002 [b]	**0.932**	0.660 (−0.023 to 0.036) [c]
Alpha	0.72 ± 0.05	0.62 ± 0.07	**<0.001**	−7.995 [a]	0.892	

The bold typeface in the table indicates the comparison with statistical significance

AUC area under the ROC curve

[a] Comparisons were performed by independent t test

[b] Comparisons were performed by Mann–Whitney U test

[c] ROC curve comparisons were conducted between ADC and the two parameters whose AUC were higher than ADC, respectively, with the 95 % confidence interval in the brackets

[d] ROC curve comparison was conducted between f and DDC with the 95 % confidence interval in the brackets using MedCalc

Fig. 1 ROC curve comparisons. In tumour and control group differentiation (**a**), there were significant differences on ROC between *f* and ADC (*P* = 0.004), between *f* and DDC (*P* = 0.010), but no difference between DDC and ADC (*P* = 0.660). In disguising the pathological subtype (**b**), no statistical difference existed between DDC and ADC (*P* = 0.958). In identifying the pathological grade of SCC (**c**) and AC (**d**), there was no statistical difference between DDC and *D* of SCC and between *D* and ADC of AC with *P* = 0.942 and 0.611
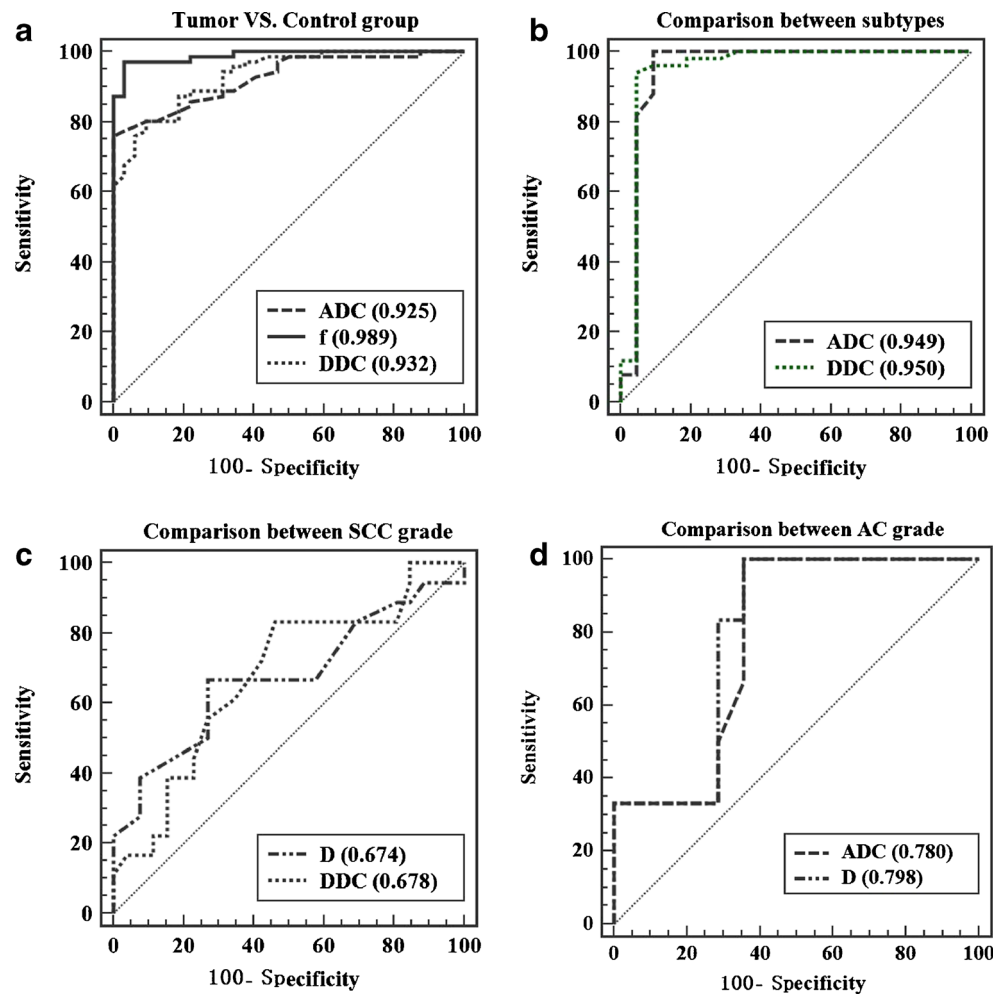
assigned taking consideration of the SNR. Great interobserver agreement was received with remarkably high ICC (0.921–0.980), supporting the reliability of the data collected, as also reported elsewhere [16, 24, 31].

Table 3 Comparison between different pathological subtypes

	SCC (*n* = 50)	AC (*n* = 21)	*P*	*t/z*	AUC	*P* value of ROC curves comparison
ADC (×10⁻³ mm²/s)	0.80 ± 0.07	1.04 ± 0.14	**<0.001**	−7.675	**0.949**	
D (×10⁻³ mm²/s)	0.62 ± 0.06	0.79 ± 0.13	**<0.001**	−5.463 [a]	0.902	
*D** (×10⁻³ mm²/s)	12.52 ± 5.39	9.11 ± 3.96	**0.011**	2.604 [a]	0.717	
f (%)	22.65 ± 3.79	30.99 ± 5.29	**<0.001**	−5.242 [b]	0.896	
DDC (×10⁻³ mm²/s)	0.85 ± 0.13	1.26 ± 0.24	**<0.001**	−5.953 [b]	**0.950**	0.958 (−0.0173 to 0.0183) [c]
Alpha	0.72 ± 0.05	0.72 ± 0.05	0.942	0.073 [a]	0.528	

The bold typeface in the table indicates the comparison with statistical significance

SCC squamous cell carcinoma, *AC* adenocarcinoma, *AUC* area under the ROC curve

[a] Comparisons were performed by independent *t* test

[b] Comparisons were performed by Mann–Whitney *U* test

[c] ROC comparison was conducted between ADC and the DDC whose AUC was higher than ADC, with the 95 % confidence interval in the bracket using MedCalc

Table 4 Comparison between different pathological grade

	SCC (n = 44)						AC (n = 20)					
	Well–moderately differentiated (n = 26)	Poorly differentiated (n = 18)	P	t/z	AUC	P value of AUC comparison	Well–moderately differentiated (n = 14)	Poorly differentiated (n = 6)	P	t/z	AUC	P value of AUC comparison [c]
ADC (×10⁻³ mm²/s)	0.82 ± 0.05	0.78 ± 0.06	0.064	1.905 [a]	–		1.08 ± 0.12	0.95 ± 0.15	**0.045**	0.374 [a]	0.780	
D (×10⁻³ mm²/s)	0.64 ± 0.04	0.61 ± 0.06	**0.037** [a]	2.155 [a]	0.674	0.942 (−0.111 to 0.119) [c]	0.82 ± 0.11	0.70 ± 0.12	**0.034**	2.292 [a]	0.798	0.611 (−0.051 to 0.087) [d]
D* (×10⁻³ mm²/s)	12.63 ± 4.53	13.01 ± 6.49	0.822 [a]	−0.227 [a]	–		9.17 ± 4.08	7.78 ± 2.52	0.454	0.765 [a]	–	
f (%)	22.24 ± 3.47	23.12 ± 3.78	0.299	−1.039 [b]	–		31.55 ± 5.64	29.95 ± 5.18	0.564	0.577 [b]	–	
DDC (×10⁻³ mm²/s)	0.88 ± 0.10	0.81 ± 0.12	**0.045** [b]	2.005 [b]	0.678		1.34 ± 0.22	1.09 ± 0.23	0.058	1.897 [b]	–	
Alpha	0.72 ± 0.04	0.72 ± 0.05	0.841	−0.201 [a]	–		0.72 ± 0.05	0.74 ± 0.04	0.368	−0.923 [a]	–	

The bold typeface in the table indicates the comparison with statistical significance

SCC squamous cell carcinoma, AC adenocarcinoma, AUC area under the ROC curve

[a] Comparisons were performed by independent t test

[b] Comparisons were performed by Mann–Whitney U test

[c] ROC curve comparison was conducted between D and DDC with the 95 % confidence interval in the bracket using MedCalc

[d] ROC curve comparison between D and ADC with the 95 % confidence interval in the bracket using MedCalc
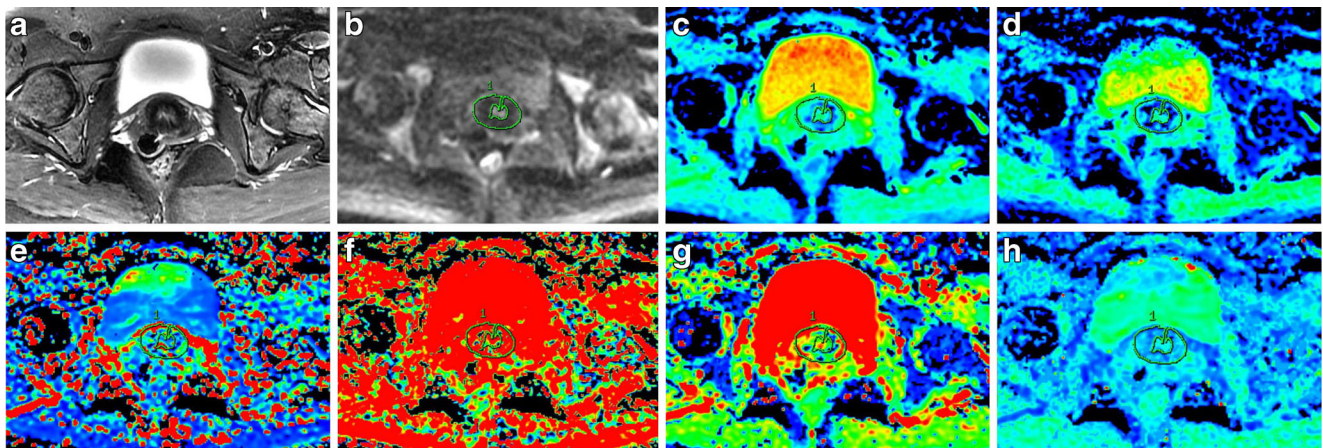
Fig. 2 Normal cervix of a 42-year-old female healthy volunteer. Axial T2-weighted image with fat suppression (**a**) showed cervical mucosa with high signal intensity and stroma with low signal intensity. Image with *b* value of 1000 s/mm^2 (**b**) The ROI encompassed all the cervix stroma (excluding the cervical mucosa). ADC, D, D*, f, DDC and alpha maps (**c–h**) from multi-*b*-value DWI-calculated mean values for the normal cervix were 1.09×10^{-3} mm^2/s, 0.66×10^{-3} mm^2/s, 32.20×10^{-3} mm^2/s, 51.50 %, 1.43×10^{-3} mm^2/s and 0.52, respectively

Mono-exponential model

ADC from MEM measures the overall diffusion level, which is mainly attributed to the cellular density that represents the ratio of extracellular to intracellular space. Comparing to the normal tissues, malignant tumour cell growth resulted in elevated level of cellular density, shrunk extracellular space and higher nuclear/cytoplasmic ratio, which would lead to lowered ADC (cervical carcinoma vs normal cervical stroma, 0.88–1.12×10^{-3} mm^2/s vs 1.50–1.72×10^{-3} mm^2/s) [3–5, 21]. Our results were consistent with previous studies in that ADC measurements were remarkably lower in cervical carcinoma than those of normal cervical stroma ($0.87 \times 10^{-3}$ mm^2/s vs 1.19×10^{-3} mm^2/s). However, we found the ADC of normal cervix in our study to be lower than those in previous studies, possibly as a result of the higher *b* value used (up to 2000 s/mm^2).

The tumour grade of cervical carcinoma conveys important prognostic information. For higher grade tumours, increased cellular density, enlarged nuclei, hyperchromatism and higher nuclear-to-cytoplasmic ratio may lead to significant decrease in ADC [6], and significant negative correlations between tumour ADC and tumour grade have been previously reported [3, 6]. However, one remaining unclarified factor in the previous studies is the subdivision of AC and SCC, which was not done as a result of the usually small number of AC cases. AC type features a higher ADC compared to that of SCC with an overlapping range [3, 5–7]. Hence the correlation between ADC and tumour
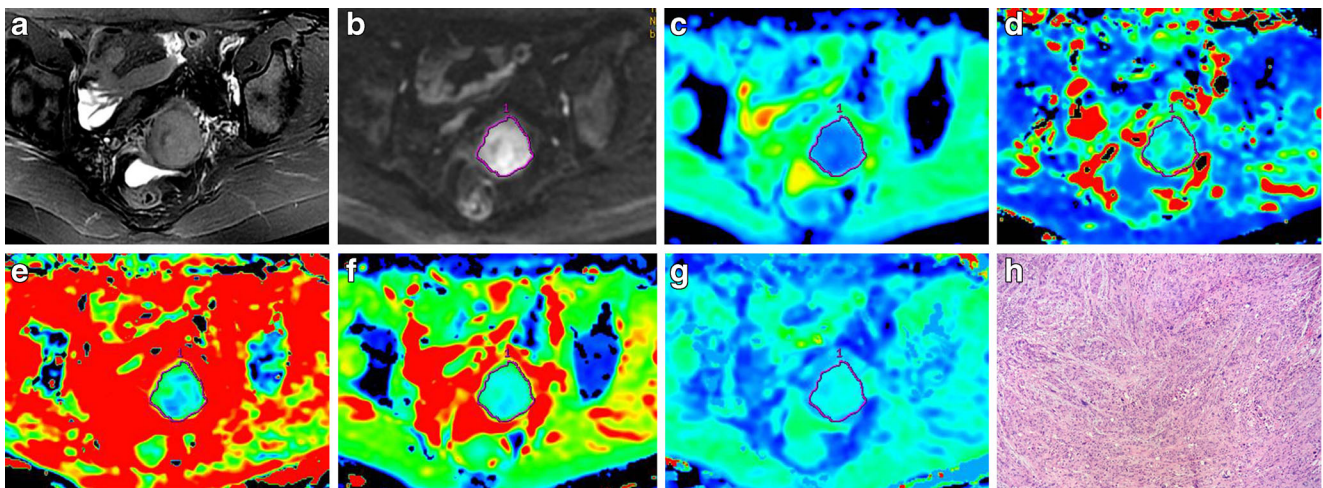
Fig. 3 A 52-year-old woman with cervical poorly differentiated squamous cell carcinoma. Axial T2-weighted image with fat suppression (**a**) showed a lobulated mass with high signal intensity. Image with *b* value of 1000 s/mm^2 (**b**) showed the ROI encompassed the whole tumour on this slice. D, D*, f, DDC and alpha maps (**c–g**) from multi-*b*-value DWI-calculated mean values for tumour were 0.61×10^{-3} mm^2/s, 8.22×10^{-3} mm^2/s, 23.6 %, 0.91×10^{-3} mm^2/s and 0.70, respectively. Histological specimen (**h**) revealed poorly differentiated cervical squamous cell carcinoma (haematoxylin–eosin stain; original magnification, ×100), which showed solid proliferation of tumour cells
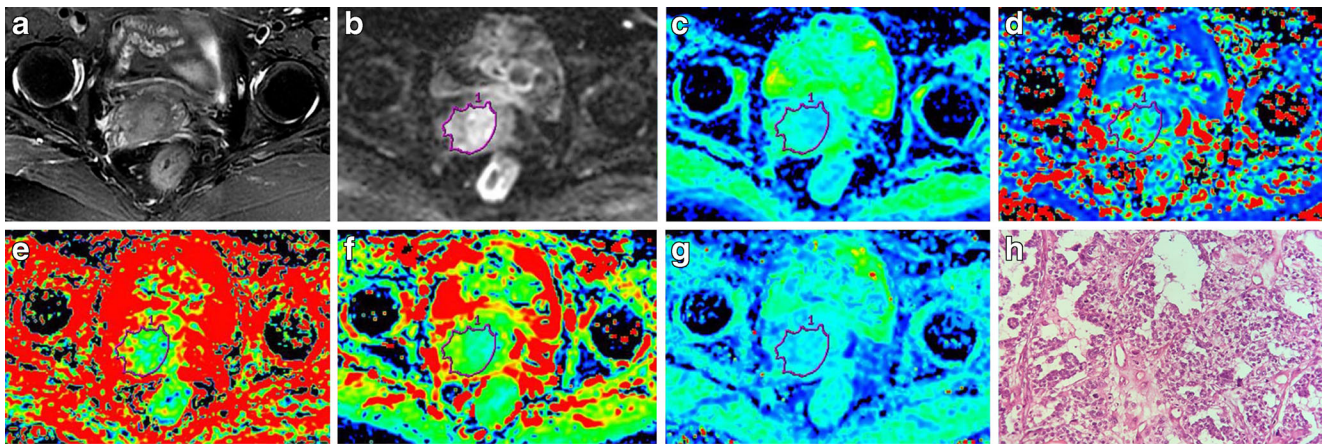
Fig. 4 A 67-year-old woman with cervical poorly differentiated adenocarcinoma. Axial T2-weighted image with fat suppression (**a**) showed a lobulated mass with high signal intensity. Image with *b* value of 1000 s/mm^2 (**b**) showed the ROI encompassed the whole tumour on this slice. *D, D*, f,* DDC and alpha maps (**c–g**) from multi-*b*-value DWI-calculated mean values for the tumour were 0.74×10^{-3} mm^2/s, 10.60×10^{-3} mm^2/s, 29.20 %, 1.20×10^{-3} mm^2/s and 0.69, respectively. Histological specimen (**h**) revealed poorly differentiated cervical adenocarcinoma (haematoxylin–eosin stain; original magnification, ×100), which showed mainly solid components with scattered neoplastic glands

grades with samples including both AC and SCC may be affected by the portion of AC cases. In this present study, the tumour cases were subdivided into SCC and AC groups and analysed separately. In past studies, it has been reported that significant differences existed between the ADCs of well/moderately differentiated tumours and poorly differentiated tumours for SCC, such as by Payne et al. [5] and Kuang et al. [7]; however, no previous report on grade differentiation for AC has been made. In this study, ADC was seen to have a weak correlation (*P* = 0.045) with tumour grade in AC (1.08×10^{-3} mm^2/s vs 0.95×10^{-3} mm^2/s). Hence the ability of ADC in differentiating grades may require the support of further evidence.

Although AC only accounts for a small portion of cervical carcinoma (less than 15 %) [32], it features poorer response to radiotherapy and worse prognosis than SCC. Therefore the subcategorizing of cervical carcinoma is important for therapeutic decisions and predicting outcomes. The physiological distinction between AC and SCC is the increased mucus secretion, which may impact the diffusion. In this study a lower mean ADC of SCC was observed as compared to AC (0.80×10^{-3} mm^2/s vs 1.04×10^{-3} mm^2/s), which is consistent with previous reports ($0.85/0.87/0.80$ [$\times 10^{-3}$ mm^2/s] vs $0.98/1.11/1.01$ [$\times 10^{-3}$ mm^2/s] [3, 6, 7]).

Bi-exponential model

BEM allows the separation of the diffusion and perfusion component from overall DWI measurements [33, 34]. As a result, the *D* value that measures the pure diffusion would be
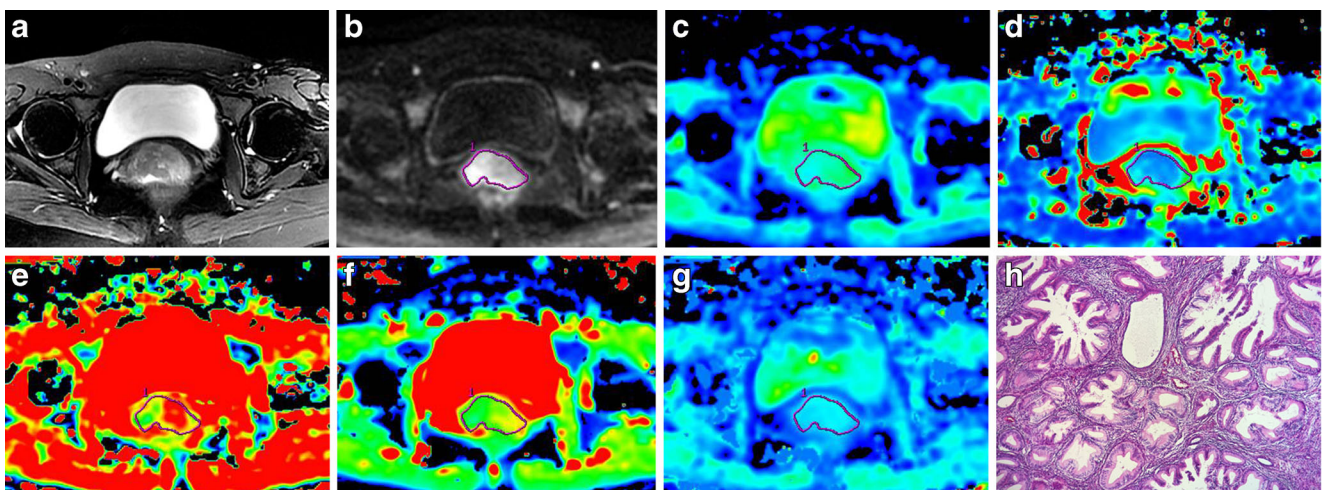
Fig. 5 A 25-year-old woman with cervical well-differentiated adenocarcinoma. Axial T2-weighted image with fat suppression (**a**) showed an irregular mass with high signal intensity. Image with *b* value of 1000 s/mm^2 (**b**) showed the ROI encompassed the whole tumour on this slice. *D, D*, f,* DDC and alpha maps (**c–g**) from multi-*b*-value DWI-calculated mean values for the tumour were 0.88×10^{-3} mm^2/s, 6.01×10^{-3} mm^2/s, 37.70 %, 1.55×10^{-3} mm^2/s and 0.75, respectively. Histological specimen (**h**) revealed well-differentiated cervical adenocarcinoma (haematoxylin–eosin stain; original magnification, ×100), which showed multiple neoplastic glands

lower than the ADC value. Similar to the observation made with ADC, a lower D value was also obtained in cervical carcinoma than those in normal cervical stroma (0.67×10^{-3} mm^2/s vs 0.77×10^{-3} mm^2/s); also a consistently lower D value was obtained in SCC than AC (0.62×10^{-3} mm^2/s vs 0.78×10^{-3} mm^2/s).

D^* represents a perfusion-related coefficient and reflects the capillary blood velocity [34]. No statistical difference between cervical carcinoma and normal cervix was reported in a study by Lee et al. (71.30×10^{-3} mm^2/s vs 69.41×10^{-3} mm^2/s) [21]. However in the present study, D^* was seen to be lower in cervical carcinoma than normal cervix, and also showed statistically significant difference between pathological subtypes (higher in SCC than AC). This also indicates that D^* is not the dominating factor in ADC, since ADC of SCC was lower than that of AC as discussed. A shortcoming of D^* is its repeatability, potentially because of the limited small b value range of measurements available [16, 21, 27]. It was also observed in this study that D^* showed higher standard deviation, lowest consistency (0.921, with relatively wide confidence interval) and higher P value (0.011 between subtypes) among all parameters measured.

The parameter f from BEM is known to be generally correlated with the fractional volume of capillary blood flowing and blood vessel density [35]. Based on literature, the microvessel density (MVD) values were 66, 31 and 53 microvessels per mm^2 in tumour periphery, tumour core and normal cervix, respectively; moreover the MVD of the tumour core decreased with larger tumour size [36]. The relationship between the MVD of the entire tumour and normal cervix remains unclear as a result of the influence of tumour sizes; significantly lower f measurements based on ROIs enclosing the entire tumour were seen in carcinoma as compared to those of normal cervix, which is consistent with previous studies of cervix [21], prostate [35, 37] and pancreas [18, 38]. It was also observed in this study that AC had a higher f as compared to SCC, and this is consistent with the pathological evidence that AC is associated with higher MVD than SCC [39].

Stretched exponential model

Alpha describes the deviation of water diffusion from a single exponential decay. Generally, tumours are believed to have higher cellular and glandular pleomorphism than normal tissue, resulting in a higher level of intravoxel diffusion heterogeneity that leads to a lower alpha [26]. A lower alpha of normal cervix than that of tumours was seen in this study, which could be explained by the anisotropy of the fibrous tissue in normal cervix that leads to comparatively more heterogeneous diffusion than in tumour. This could be similar to the case of white matter that is highly anisotropic and shows lower ADC and alpha than grey matter [40, 41]. A previous

study also reported significance of alpha in predicting tumour grade in glioma [24], but no difference was noted in grade of cervical carcinoma in this study; hence, further study would be needed for this investigation.

There is strong correlation between ADC and DDC in tumours [24, 26, 42]. Theoretically, when $\alpha = 1$, DDC is equivalent to mono-exponential diffusion-weighted signal decay reflecting low intravoxel diffusion heterogeneity; when $\alpha = 0$, DDC signifies high intravoxel diffusion heterogeneity related to multi-exponential decay. The study by Liu et al. [26] indicated that the mean DDC value was higher than the ADC in normal tissues but lower than the ADC in prostate carcinoma. However, in this study the DDC values of normal cervix and cervical carcinoma were both higher than ADC, which was consistent with the study on brain tumour [42]. In addition, DDC showed the same tendency as ADC and D value in distinguishing tumour and normal cervix, pathological subtype and grade of SCC, which was consistent with the study on gliomas [24]. The reduction in DDC can be explained by more intravoxel diffusion heterogeneity between tumour and normal tissue, and between different tumour grades.

Comparison between models

Parameters derived from MEM, BEM and SEM are related but provide diversified information. Previous studies showed that ADC value was positively related to stage of cervical carcinoma, as well as bi-exponential parameters in NPC [25, 43], while no correlation was found between the intravoxel diffusion-related parameters and tumour stage in this study. All the parameters showed statistically significant difference in tumour diagnosis, and the f value derived from BEM featured the best performance with the highest AUC of 0.989 (higher than ADC by MEM and DDC by SEM). For distinguishing pathological subtypes, DDC showed the highest AUC but demonstrated indifferent statistical difference to ADC (0.950 vs 0.949). Our results also showed that DDC and ADC were related to tumour grade on SCC and AC, respectively, with weak statistical difference (both $P = 0.045$), while only D value could differentiate tumour grade both in SCC ($P = 0.037$) and AC ($P = 0.034$), which indicated that D values have better ability to predict tumour grade.

Limitations

There were several limitations in this study. Firstly, there was a lack of pathological comparison, such as MVD, which is commonly used as a surrogate marker of angiogenesis. Secondly, the relatively small cohort of AC made individual comparisons among three differentiation grades infeasible. Finally, the collection of SCC and AC data was over different time periods as a result of hospital schedules; however, consecutive enrolment and sufficient sample size were ensured for both cases.

Conclusion

In this study, we investigated the use of three DWI models, MEM, BEM and SEM, in cervical carcinoma. Overall, it was seen that the additional parameters derived from BEM and SEM, in addition to the ADC from MEM, showed reliability and feasibility in clinical use for cervical carcinoma. Hence multi-*b*-value DWI acquisitions would be desirable in practice, bearing the cost of additional scan time. The non-invasive nature of DWI and the diverse clinical information available by choosing appropriate models hold great promise in the tumour diagnosis, subtype and grade evaluation, and further research is needed.

References

1. Follen M, Levenback CF, Iyer RB et al (2003) Imaging in cervical cancer. Cancer 98:2028–2038

2. Nicolet V, Carignan L, Bourdon F, Prosmanne O (2000) MR imaging of cervical carcinoma: a practical staging approach. Radiographics 20:1539–1549

3. Liu Y, Bai R, Sun H, Liu H, Wang D (2009) Diffusion-weighted magnetic resonance imaging of uterine cervical cancer. J Comput Assist Tomogr 33:858–862

4. Demirbas T, Cimilli T, Bayramoglu S, Guner NT, Hocaoglu E, Inci E (2014) Contribution of diffusion-weighted imaging to diagnosis and staging of cervical cancer. Balkan Med J 31:154–157

5. Payne GS, Schmidt M, Morgan VA et al (2010) Evaluation of magnetic resonance diffusion and spectroscopy measurements as predictive biomarkers in stage 1 cervical cancer. Gynecol Oncol 116:246–252

6. Liu Y, Ye Z, Sun H, Bai R (2015) Clinical application of diffusion-weighted magnetic resonance imaging in uterine cervical cancer. Int J Gynecol Cancer 25:1073–1078

7. Kuang F, Ren J, Zhong Q, Liyuan F, Huan Y, Chen Z (2013) The value of apparent diffusion coefficient in the assessment of cervical cancer. Eur Radiol 23:1050–1058

8. Andersen EK, Hole KH, Lund KV et al (2013) Pharmacokinetic parameters derived from dynamic contrast enhanced MRI of cervical cancers predict chemoradiotherapy outcome. Radiother Oncol 107:117–122

9. Himoto Y, Fujimoto K, Kido A et al (2014) Assessment of the early predictive power of quantitative magnetic resonance imaging parameters during neoadjuvant chemotherapy for uterine cervical cancer. Int J Gynecol Cancer 24:751–757

10. Ellingsen C, Hompland T, Galappathi K, Mathiesen B, Rofstad EK (2014) DCE-MRI of the hypoxic fraction, radioresponsiveness, and metastatic propensity of cervical carcinoma xenografts. Radiother Oncol 110:335–341

11. Federau C, O'Brien K, Meuli R, Hagmann P, Maeder P (2014) Measuring brain perfusion with intravoxel incoherent motion (IVIM): initial clinical experience. J Magn Reson Imaging 39:624–632

12. Woo S, Lee JM, Yoon JH, Joo I, Han JK, Choi BI (2014) Intravoxel incoherent motion diffusion-weighted MR imaging of hepatocellular carcinoma: correlation with enhancement degree and histologic grade. Radiology 270:758–767

13. Fujima N, Yoshida D, Sakashita T et al (2014) Intravoxel incoherent motion diffusion-weighted imaging in head and neck squamous cell carcinoma: assessment of perfusion-related parameters compared to dynamic contrast-enhanced MRI. Magn Reson Imaging 32:1206–1213

14. Bisdas S, Braun C, Skardelly M et al (2014) Correlative assessment of tumor microcirculation using contrast-enhanced perfusion MRI and intravoxel incoherent motion diffusion-weighted MRI: is there a link between them? NMR Biomed 27:1184–1191

15. Lee EY, Hui ES, Chan KK et al (2015) Relationship between intravoxel incoherent motion diffusion-weighted MRI and dynamic contrast-enhanced MRI in tissue perfusion of cervical cancers. J Magn Reson Imaging 42:454–459

16. Orton MR, Messiou C, Collins D et al (2016) Diffusion-weighted MR imaging of metastatic abdominal and pelvic tumours is sensitive to early changes induced by a VEGF inhibitor using alternative diffusion attenuation models. Eur Radiol 26:1412–1419

17. Jia QJ, Zhang SX, Chen WB et al (2014) Initial experience of correlating parameters of intravoxel incoherent motion and dynamic contrast-enhanced magnetic resonance imaging at 3.0 T in nasopharyngeal carcinoma. Eur Radiol 24:3076–3087

18. Lemke A, Laun FB, Klauss M et al (2009) Differentiation of pancreas carcinoma from healthy pancreatic tissue using multiple b-values: comparison of apparent diffusion coefficient and intravoxel incoherent motion derived parameters. Investig Radiol 44:769–775

19. Chandarana H, Lee VS, Hecht E, Taouli B, Sigmund EE (2011) Comparison of biexponential and monoexponential model of diffusion weighted imaging in evaluation of renal lesions: preliminary experience. Investig Radiol 46:285–291

20. Liu C, Liang C, Liu Z, Zhang S, Huang B (2013) Intravoxel incoherent motion (IVIM) in evaluation of breast lesions: comparison with conventional DWI. Eur J Radiol 82:e782–e789

21. Lee EY, Yu X, Chu MM et al (2014) Perfusion and diffusion characteristics of cervical cancer based on intraxovel incoherent motion MR imaging-a pilot study. Eur Radiol 24:1506–1513

22. Bennett KM, Schmainda KM, Bennett RT, Rowe DB, Lu H, Hyde JS (2003) Characterization of continuously distributed cortical water diffusion rates with a stretched-exponential model. Magn Reson Med 50:727–734

23. Bennett KM, Hyde JS, Schmainda KM (2006) Water diffusion heterogeneity index in the human brain is insensitive to the orientation of applied magnetic field gradients. Magn Reson Med 56:235–239

24. Bai Y, Lin Y, Tian J et al (2015) Grading of gliomas by using monoexponential, biexponential, and stretched exponential

diffusion-weighted MR imaging and diffusion kurtosis MR imaging. Radiology 278:496–504

25. Lai V, Lee VH, Lam KO, Sze HC, Chan Q, Khong PL (2015) Intravoxel water diffusion heterogeneity MR imaging of nasopharyngeal carcinoma using stretched exponential diffusion model. Eur Radiol 25:1708–1713

26. Liu X, Zhou L, Peng W, Wang H, Zhang Y (2015) Comparison of stretched-exponential and monoexponential model diffusion-weighted imaging in prostate cancer and normal tissues. J Magn Reson Imaging 42:1078–1085

27. Mazaheri Y, Afaq A, Rowe DB, Lu Y, Shukla-Dave A, Grover J (2012) Diffusion-weighted magnetic resonance imaging of the prostate: improved robustness with stretched exponential modeling. J Comput Assist Tomogr 36:695–703

28. Merisaari H, Toivonen J, Pesola M et al (2015) Diffusion weighted imaging of prostate cancer: effect of b-value distribution on repeatability and cancer characterization. Magn Reson Imaging 33:1212–1218

29. Winfield JM, deSouza NM, Priest AN et al (2015) Modelling DW-MRI data from primary and metastatic ovarian tumours. Eur Radiol 25:2033–2040

30. Merisaari H, Jambor I (2015) Optimization of b-value distribution for four mathematical models of prostate cancer diffusion-weighted imaging using b values up to 2000 s/mm(2): simulation and repeatability study. Magn Reson Med 73:1954–1969

31. Matoba M, Tonami H, Kondou T et al (2007) Lung carcinoma: diffusion-weighted MR imaging–preliminary evaluation with apparent diffusion coefficient. Radiology 243:570–577

32. Kaur H, Silverman PM, Iyer RB, Verschraegen CF, Eifel PJ, Charnsangavej C (2003) Diagnosis, staging, and surveillance of cervical carcinoma. AJR Am J Roentgenol 180:1621–1631

33. Le Bihan D, Breton E, Lallemand D, Grenier P, Cabanis E, Laval-Jeantet M (1986) MR imaging of intravoxel incoherent motions: application to diffusion and perfusion in neurologic disorders. Radiology 161:401–407

34. Le Bihan D (2008) Intravoxel incoherent motion perfusion MR imaging: a wake-up call. Radiology 249:748–752

35. Shinmoto H, Tamura C, Soga S et al (2012) An intravoxel incoherent motion diffusion-weighted imaging study of prostate cancer. AJR Am J Roentgenol 199:W496–W500

36. Hockel S, Schlenger K, Vaupel P, Hockel M (2001) Association between host tissue vascularity and the prognostically relevant tumor vascularity in human cervical cancer. Int J Oncol 19:827–832

37. Shinmoto H, Oshio K, Tanimoto A et al (2009) Biexponential apparent diffusion coefficients in prostate cancer. Magn Reson Imaging 27:355–359

38. Lee SS, Byun JH, Park BJ et al (2008) Quantitative analysis of diffusion-weighted magnetic resonance imaging of the pancreas: usefulness in characterizing solid pancreatic masses. J Magn Reson Imaging 28:928–936

39. Tokumo K, Kodama J, Seki N et al (1998) Different angiogenic pathways in human cervical cancers. Gynecol Oncol 68:38–44

40. Nicolas R, Sibon I, Hiba B (2015) Accuracies and contrasts of models of the diffusion-weighted-dependent attenuation of the MRI signal at intermediate b-values. Magn Reson Insights 8:11–21

41. Grech-Sollars M, Hales PW, Miyazaki K et al (2015) Multi-centre reproducibility of diffusion MRI parameters for clinical sequences in the brain. NMR Biomed 28:468–485

42. Kwee TC, Galban CJ, Tsien C et al (2010) Comparison of apparent diffusion coefficients and distributed diffusion coefficients in high-grade gliomas. J Magn Reson Imaging 31:531–537

43. Lai V, Li X, Lee VH et al (2014) Nasopharyngeal carcinoma: comparison of diffusion and perfusion characteristics between different tumour stages using intravoxel incoherent motion MR imaging. Eur Radiol 24:176–183